



LAWRENCE
LIVERMORE
NATIONAL
LABORATORY

Droplet Evolution in Warm Dense Matter Expanding Flow

J. Armijo, J. J. Barnard

September 16, 2010

Physical Review E

Disclaimer

This document was prepared as an account of work sponsored by an agency of the United States government. Neither the United States government nor Lawrence Livermore National Security, LLC, nor any of their employees makes any warranty, expressed or implied, or assumes any legal liability or responsibility for the accuracy, completeness, or usefulness of any information, apparatus, product, or process disclosed, or represents that its use would not infringe privately owned rights. Reference herein to any specific commercial product, process, or service by trade name, trademark, manufacturer, or otherwise does not necessarily constitute or imply its endorsement, recommendation, or favoring by the United States government or Lawrence Livermore National Security, LLC. The views and opinions of authors expressed herein do not necessarily state or reflect those of the United States government or Lawrence Livermore National Security, LLC, and shall not be used for advertising or product endorsement purposes.

Droplet Evolution in Warm Dense Matter Expanding Flow

J. Armijo*

Lawrence Berkeley National Laboratory, Berkeley, CA 94720, USA

J.J. Barnard

Lawrence Livermore National Laboratory, Livermore, CA 94550, USA

(Dated: August 25, 2010)

We propose a simple kinetic model for the evolution of a droplet in a cell, based on the Van der Waals equation of state, to investigate the behavior of a mixture of liquid and vapor undergoing adiabatic expansion in vacuum after rapid, isochoric heating. We study the evolution of the two-phase fluid at intermediate times between the molecular and the hydrodynamic scales, focussing on out-of-equilibrium and surface effects. We find a formula for the temperature difference between the gas and the droplets and we check it with numerical calculations. We then use the formula to delimit the thermalized and non-thermalized regimes of expansion. In the thermalized case, the liquid fraction grows in a proportion that we estimate analytically, whereas, in case of too rapid expansion, a strict limit for the evaporation of droplets is derived. The range of experimental situations is discussed.

PACS numbers: 51.10.+y, 64.70.fm

I. INTRODUCTION

Warm Dense Matter (WDM) conditions (density $0.01 \rho_{solid} < \rho < \rho_{solid}$ and temperature $0.1\text{eV} < T < 10\text{eV}$) can be defined as the region of thermodynamic space corresponding to the double crossover from degenerate to non-degenerate and from weakly to strongly coupled matter [1], so that the “easy” limiting descriptions in terms of cool plasma and hot condensed matter meet and have to be somehow connected to each other. This problem is drawing growing attention because of the serious theoretical challenges involved, and because of the occurrence of WDM in the contexts of Inertial Fusion Energy (IFE), astrophysics (planet cores), and laser ablation for materials processing, nanoparticles formation and film deposition [2–4].

Most of these situations involve rapid heating of a material, which means that the energy deposition (by lasers, ions, neutrons, electrical discharges, etc.) is much faster than its release through hydrodynamic expansion. Pressures in the kbar to Mbar range are reached before giving rise to supersonic expansion with typical outflow velocities of several km/s.

During such expansion and adiabatic cooling, it is almost inevitable that the material enters at some point into the two-phase region of the phase diagram. This happens either from below the critical point (ion heating experiments such as GSI in Darmstadt [5, 6], or NDCX II at LBNL [7], low fluence laser ablation, Z machines), or from above it (IFE, high fluence laser ablation, upcoming ion heating machines). In the first case an over-stretched liquid fragments and evaporates into a mixture of droplets and gas, whereas in the second case a hot supersaturated gas nucleates small clusters while expanding. In both cases the flow becomes a *plume* of gas and

condensed clusters, meaning that a monophasic fluid has undergone phase separation with the creation of surfaces giving a non-trivial geometry to the fluid, which may a priori affect its dynamical properties.

Recently, there has been significant progress in the observation of those two-phase flows, from the early ablation and plume expansion stages in the ps and ns timescales [8–11] to the late μs timescale evolution including “post-mortem” analysis of the clusters [12, 13].

Basic questions arise when considering a two-phase flow. First, such flow is a mixture of gas and clusters (most often liquid, so the term “droplet” is appropriate), so one may ask: what is the droplets’ size and distribution, and how do they evolve during the expansion? A second important question concerns the temperature of the gas and drops: is there equilibrium? The answer can determine the conditions of validity for hydrodynamic approaches based on the Maxwell Construction or any two-phase Equation of State (EoS) that assumes local equilibrium.

So far, two main approaches have been used. On one hand, Molecular Dynamics (MD) codes [14–20] compute the dynamics of each particle separately, and have given powerful insight into the processes of fragmentation, phase explosion, and the different mechanisms for ablation, but they are inherently limited to only treat the early times ($< 1\text{ns}$, [50]), and with a small number of particles ($\sim 10^7$). On the other hand, hydrodynamic codes [13, 21–24] can model experiments completely, but they deal with mesoscopic fluid cells, and often rely on crude approximations concerning the molecular and kinetic processes involved. Complex hydrodynamic codes including a treatment of the kinetics of phase change processes and surface effects in each cell are under development [13, 25], but providing a complete and reliable description of a whole WDM experiment is still a challenge.

Better understanding of two-phase flows should be helpful for the preparation of experiments, including the diagnostics, and for the interpretation of the data. In IFE especially, the problem of debris dynamics is a crucial issue due to their impact on the optics and other components of the target chambers [25, 26].

In this paper we propose a simple model to study two-phase flows in WDM situations. Our model was initially conceived to predict the phenomenology of the upcoming target heating experiments with the NDCX II machine at LBNL where an ion beam will almost isochorically heat a thin metallic foil to temperatures of about 1eV. However, the model should apply to any two-phase flow.

For the EoS, we use the Van der Waals fluid model, which allows us to build a complete set of thermodynamic functions needed for our computation. The particle and energy fluxes between a drop and the surrounding gas are described with a self-consistent set of kinetic rate equations, that is original to our knowledge. The computing cell is considered as part of a larger hydrodynamic code, but in this paper we only consider one cell containing one droplet. We use our model to distinguish the different regimes of two-phase expansion: on one side, quasi or fully-thermalized, on the other side, non-thermalized. We show that this distinction depends on the initial target dimensions and the initial temperature. We then study those regimes analytically and numerically.

II. BACKGROUND

A. Expanding two-phase flows. Supercritical and subcritical cases

The model that we propose lies at a mesoscopic scale between the molecular and hydrodynamic scales, so we need some preliminar assumptions. Our computing cell is considered as an elementary piece of a larger hydrodynamic code describing an expanding flow. The linear strain rate η characterizes the expansion of the cell $L = L_0(1 + \eta t)$, where L_0 is the initial cell size. We define the hydrodynamic timescale $t_{hydro} = \eta^{-1}$. In the following, we assume rapid heating ($t_{heating} < t_{hydro}$) so that the energy deposition in the material is almost isochoric. For simplicity, we will assume instantaneous energy deposition. In Table I, we gather the most relevant parameters of our model and, for some, their values in the reference case considered throughout this paper.

To get insight into the global flow, it is interesting to review some analytical and numerical results. The Self Similar Rarefaction Wave (SSRW) is the solution [27] describing the 1D expansion of a perfect gas (semi-infinite at $z < 0$) of adiabatic coefficient γ after instantaneous uniform heating. In this solution the outward expanding front travels at $2cs_0/(\gamma - 1)$, which is $3cs_0$ for a perfect monoatomic gas, while the inward rarefaction wave prop-

T_0	initial temperature	8000K
δz	initial foil thickness	$3.5\mu\text{m}$
δr	beam diameter	1mm
cs_0	sound speed at T_0	
v_0	$3cs_0$: outflow velocity	5km/s
η_z	$2v_0/\delta z$: axial strain rate	
η_r	$2v_0/\delta r$: radial strain rate	
$\tilde{\eta}$	$d(V/V_0)/dt$: volume strain rate	
t_{hydro}	η_z^{-1} : hydrodynamic time	0.37ns
t_{3D}	η_r^{-1} : time for crossover to 3D expansion regime	100ns
R_0	initial droplet radius	20nm
L_0, V_0	initial cell size, volume	
a	VdW interaction parameter	
b	VdW volume per particle	
l_0	a/b: latent heat at $T = 0$ per atom	3.07eV
θ	$k_B T/l_0$: reduced temperature	
$n_{l,g}$	particle densities	
n_g^*	equilibrium gas density	
$v_{l,g}$	volumes per particle	
$e_{l,g}$	energies per particle	
$E_{l,g}$	total energies in the cell	
σ	surface tension	
$\Phi_{vap,cond}$	evaporation, condensation fluxes	
α	thermalization coefficient	0.5
β	condensation (sticking) coefficient	0.5
x	N_l/N_{tot} : liquid fraction in the cell	

TABLE I: Relevant parameters for the model and typical values in the NDCXII reference case

agates at cs_0 [23]. Note that the SSRW can be computed semi-numerically for any EoS of a non-ideal gas [28] and has been validated by MD simulations [18].

As an example of a numerical simulation of expanding flows, Figure 1 shows a hydrodynamic calculation with the code DPC using an EoS based on Maxwell Construction [22]. Here the liquid and gas are assumed in equilibrium, which is not kinetically justified (see Section IV.B), and the outflow velocity is about 8km/s after 10ns.

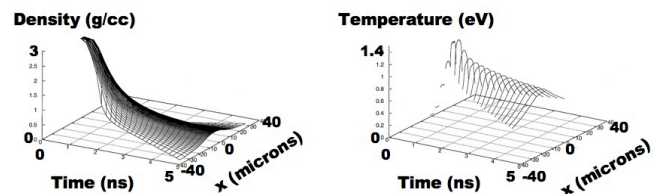


FIG. 1: Hydrodynamic calculation with DPC code of NDCX II reference case, from [23]. A $3.5\mu\text{m}$ -thick Al foil is heated within 1ns with an ion beam and subsequently cools down during adiabatic expansion

In the following we will assume a flow with linear speed profile and outflow velocity $v_0 = 3cs_0$, but it is worth remarking that this is quite simplistic. In particular, several numerical works [21, 23, 28] have reported the occurrence of "plateaus", i.e. zones of nearly constant density, related to the fluid zones entering into the two-phase regime.

When mapping the calculation of Fig. 1 onto the corresponding phase diagram, one sees that the material first melts, and then expands and crosses the liquid binodal, thus undergoing fragmentation, which we call the *subcritical case*. If the material was initially heated to higher temperatures, it would instead expand first as a supercritical fluid and pass the critical point from above, thus reaching the two-phase region at lower densities, when crossing the gas binodal. Nucleation of small droplets can then occur. We call it the *supercritical case*.

Figure 2 represents the two cases and the various experimental situations that they involve. On Fig. 2.a, we show the Van der Waals phase diagram for Aluminum that we use in the following, and a schematical representation of the sub- and supercritical cases of two-phase expansion (arrow 1 and 2). On Fig. 2.b, reproduced from [17], one sees the non-uniform particle distribution in a 2D MD simulation of laser ablation. One can distinguish the different regimes from unablated dense phase (I) to dense material undergoing cavitation and fragmentation (II), mixture of fragmented material and vaporized material having recondensed (III) and fully atomized gas (IV). In our classification, zone II is a two-phase flow in the subcritical case, zone III is a mixture of sub- and supercritical cases, and zone IV is an expanding gas that is likely to reach the two-phase boundary in the supercritical case. The four stages of the MD evolution are placed qualitatively on Fig. 2.a.

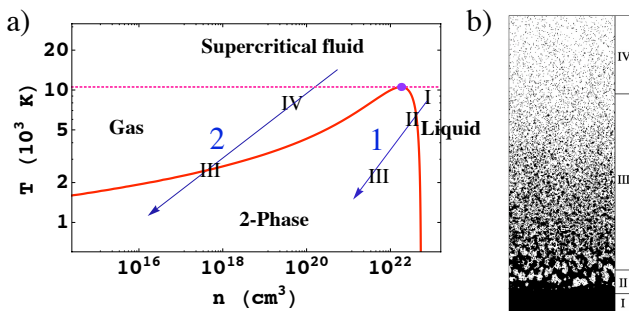


FIG. 2: a) Phase diagram of the Van der Waals EoS for Al (see Section III) showing the liquid and gas binodals (solid lines), and a schematical representation of the sub- (arrow 1) and supercritical (arrow 2) cases of two-phase expansion. b) 2D MD simulation of laser ablation with inhomogeneous initial temperature, from [17], showing which material in various situations of two-phase expansion, which we also locate qualitatively on Fig. 2.a (roman numbers).

B. Initial droplet size

Both cases lead to droplets formation. In order to initialize the kinetic model that we present further, it is necessary to know the initial droplet size at the onset of the two-phase regime.

In the subcritical case, the overstretched liquid starts cavitating (see Fig. 2.b, zone II), which we call the *bubbles regime* and then the bubbles percolate until the liquid phase is not continuous anymore (see Fig. 2.b, zone III), which we call the *droplets regime*. We assume that the droplets regime starts when the gas and liquid volumes are equal: $V_g = V_l$, which is justified by an argument of surface energy minimization.

The mean droplet's size in a fragmentation scenario can be obtained by considering a balance between the disruptive inertial forces and the restoring surface tension [14]. The model proposed initially by Grady [29] has been abundantly validated by MD calculations [14, 17, 20] in 2D and 3D, and is in very good agreement with measurements on He jets [30]. We note that the scaling of the mean radius R of the drop can be obtained by just setting to unity the Weber number $We \equiv \rho R v^2 / \sigma$ [31], where σ is the surface tension ρ the liquid mass density, and $v = \eta R$ the typical velocity difference across a piece of fluid of size R . We is the ratio of the surface energy to the inertial energy. In any dimension this criterion yields

$$We \sim 1 \Rightarrow R \sim \left(\frac{\sigma}{\rho \eta^2}\right)^{\frac{1}{3}} \quad (1)$$

Several values of order 1 have been proposed for the prefactor in this scaling law, either from analytical estimates (prefactor $15^{1/3} = 2.47$ in [24]), or from fits to MD simulation results. In [15], it was shown that both 3D MD results with a homogeneous strain rate η and data from helium free jets experiments from [30] could be fitted to Eq. 1 with the same prefactor, thus validating this law over more than 3 orders of magnitude in cluster size (the experimental fragments cover larger sizes than the numerical ones).

Concerning the size distribution of drops resulting from fragmentation, MD simulations have shown clearly that it is essentially exponential [15, 20], which is consistent with simple models of entropy maximization [14].

By contrast, it is not so clear how to describe the initial situation in the supercritical case. This task requires one to choose a model for nucleation, or to input results from MD calculations. Nucleation of clusters from a supersaturated vapor is the situation of nucleation whose kinetics is the easiest to model theoretically [32], but still choices have to be made [13], that are beyond the scope of this paper. Any model for nucleation will depend crucially on surface tension, so we make the remark here that estimating the surface tension for small droplets is delicate because of its enhancement at small sizes [33, 34].

III. MODEL

A. Van der Waals fluid model

With only two parameters, the Van der Waals (VdW) Equation of State (EoS) is the simplest EoS describing the coexistence of a liquid and a gas phase, and has already been used for theoretical studies of dynamic two-phase processes [35, 36]. All the thermodynamic functions can be derived from the expression for the mean-field potential energy per particle in such fluid: $U = +\infty$ if $n > 1/b$ and $U = -an$ if $n < 1/b$, where n is the particle density, b stands for the incompressible volume of the particles, and a represents the mean-field attractive energy between them.

The bulk VdW energy of N particles at temperature T is $E = N(c_v T - an)$. It can be shown that the specific heat c_v is independent of n and can only depend on T [37], so that one has to choose necessarily $c_v = \frac{3}{2}k_B$, where k_B is the Boltzmann constant, if one wants the EoS to match the perfect monoatomic gas in the dilute limit. Writing the partition function, one obtains the other thermodynamic functions. In particular, the pressure is $P = k_B T / (v - b) - a/v^2$ where $v = 1/n$ is the volume per particle. This expression implies that the isobars (resp. isotherms) are a cubic relationship between T and v (resp. P and v). Hence, below a certain critical temperature T_c , an unstable zone of negative compressibility appears in the phase diagram, limited by the two spinodals. We obtain the equilibrium density of the two stable phases that can coexist at certain (P, T) by numerically performing the Maxwell construction, which consists in solving $P_l = P_g$ (i) and $\mu_l = \mu_g$ (ii) simultaneously, where μ denotes the chemical potential and the subscripts l and g stand for *liquid* and *gas*, all throughout this paper. (ii) is equivalent to $\int_l^g v dP = 0$ and thus $\int_l^g P(v)dv = P_{l,g}(v_g - v_l)$ [37].

Introducing the reduced temperature $\theta = k_B T / l_0$, where $l_0 = a/b$ is the latent heat at $T = 0$, and two dimensionless parameters that are small in the low temperature limit: $v_g = b/\gamma$ and $v_l = b(1 + \delta)$, equations (i) and (ii) become:

$$\frac{\theta}{\gamma} - \frac{1}{(1 + \gamma)^2} = \frac{\theta}{\frac{1}{\delta} - 1} - \delta^2 \quad (2)$$

$$\frac{\theta \ln(\frac{1}{\delta} - 1)}{\gamma} + \delta - \frac{1}{1 + \gamma} = (\frac{\theta}{\frac{1}{\delta} - 1} - \delta^2)(\frac{1}{\delta} - (1 + \gamma)) \quad (3)$$

It is worth remarking that $T_c = 8a/27b$, so $\theta_c = 8/27 \simeq 0.3$, and therefore one expects that calculations in the "low temperature limit" ($\theta \ll 1$) should be a good approximation as soon as one is not considering the vicinity of the critical point.

Figure 3 gathers the thermodynamic functions of our VdW model for Aluminum. Fig. 3.a shows the numerical result of the dimensionless Maxwell construction where the VdW parameters $a = 9.1 \times 10^{-35} \text{erg.cm}^3$ and $b = 1.85 \times 10^{-23} \text{cm}^3$ have been adjusted to fit this material. For that, we impose that the VdW liquid density matches the aluminum liquid density $n_l(T_m) = 5.26 \times 10^{22} \text{cm}^{-3}$ at the melting point $T_m = 933.5 \text{K}$ ($= 0.026l_0$) [38] and that the VdW latent heat (shown on Fig. 3.b)

$$l = a(n_l - n_g) + P_{l,g} \left(\frac{1}{n_l} - \frac{1}{n_g} \right) \quad (4)$$

coincides with the experimental value $l(T_b) = 4.88 \times 10^{-12} \text{erg/atom}$ for Aluminum at the boiling temperature $T_b = 2792 \text{K}$ ($= 0.078l_0$) [38]. Note that the critical parameters that we obtain in this way are consistent with the best estimates to date, although not very precisely [51].

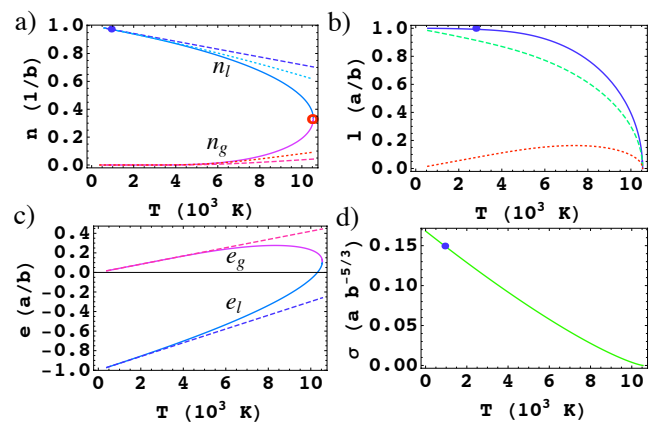


FIG. 3: Van der Waals thermodynamic functions for Aluminum, in VdW units. The dots represent experimental data and the critical point obtained from the fits. (a) Liquid and gas densities (solid lines) with first (dashed) and second order (dotted) low T approximations. (b) Latent heat (solid (dashed) and second (dotted) term of Eq. 4. (c) Bulk energies per particle, with first order low T approximations of Eq. 7 (dashed). (d) Surface tension (Eq. 8).

On Fig. 3.a are also displayed the simple, useful approximations for n_l and n_g at lowest orders in θ that one obtains directly from Eq. 2 and 3:

$$n_l \simeq \frac{1}{b}(1 - \theta - \theta^2) \quad (5)$$

$$n_g \simeq \frac{1}{b\theta} \exp\left(-\frac{1}{\theta(1 + \theta)}\right) \quad (6)$$

Note that Eq. 6 is, at lowest order in θ , equivalent to the Clausius-Clapeyron formula applied to a perfect gas. We also show on Fig 3.c the approximations at first order in θ for the liquid and gas bulk energies per particle

$$e_g \simeq \frac{3}{2}k_B T \quad ; \quad e_l \simeq \frac{5}{2}k_B T - \frac{a}{b} \quad (7)$$

For the surface tension, Van der Waals himself had already proposed to model it using density gradients [36], but we have chosen to use a simple formula that is universally verified in simple fluids [39]

$$\sigma \propto (1 + T/T_c)^{1+r} \quad \text{with} \quad r = 0.27 \quad (8)$$

To model Aluminum, we fit this formula to the experimental value $\sigma(T_m) = 1050 \text{erg/cm}^2$ [40], as shown on Fig. 3.d. Note that in the following, the total liquid energy in the cell is $E_l = N_l e_l + \sigma S_l$, where S_l is the surface area of the droplet.

B. Kinetic equations

Our goal is to compute the evolution of droplets in cells. In this paper we limit ourselves to the case of one droplet in one lagrangian cell undergoing adiabatic expansion. It is a closed system out of equilibrium, and its complete description requires the determination of the four variables N_l, n_l, T_l, T_g . To compute their evolution, we need four rate equations: a liquid-gas particle exchange rate, an energy exchange rate, a total energy loss rate (work to the outside), and an internal equilibrium condition to determine the liquid density. As shown on Fig. 4.a, the particle fluxes between liquid and gas are divided between evaporating, condensing, and condensing but not-sticking particles.

The volume expansion $V(t)$ shall later be prescribed by a global hydrodynamic code. For our study, we assume cylindrical symmetry and we use a simple model behavior [15, 16]

$$V(t) = V_0(1 + \eta_z t)(1 + \eta_r t)^2 \quad (9)$$

where η_z and η_r are the axial and radial strain rates corresponding to the beam direction and the target plane respectively. The particle fluxes between liquid and gas are computed using the standard Hertz-Knudsen formulas [41, 42]

$$\Phi_{cond} = n_g \sqrt{\frac{k_B T_g}{2\pi m}} \quad ; \quad \Phi_{vap} = n_g^*(T_l, R) \sqrt{\frac{k_B T_l}{2\pi m}} \quad (10)$$

where $n_g^*(T_l, R)$ is the *equilibrium gas density* for a drop at temperature T_l and of radius R . To estimate n_g^* , we use the Kelvin equation, which describes the increase of the equilibrium vapor pressure surrounding a drop due to surface tension

$$n_g^*(R) = n_g^*(\infty) \exp\left(\frac{2\sigma}{k_B T n_l R}\right) \quad (11)$$

Kelvin equation is approximate because its derivation assumes a perfect gas. Also, we use a constant value for σ , thus neglecting its increase at small radii [33, 34]. Still, this approach is probably not too bad after all [43], and satisfactory enough for our qualitative purpose.

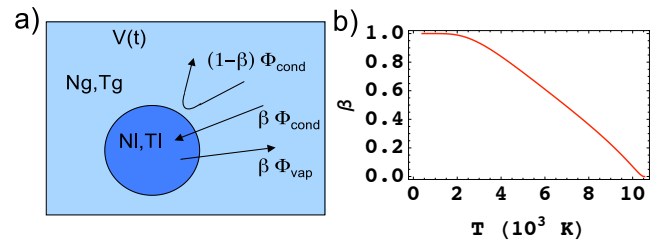


FIG. 4: The "drop-in-cell" kinetic model. a) Sketch of the kinetic fluxes. b) Sticking coefficient β calculated with formula from [44] and our aluminum VdW parameters.

Considering mass conservation, and combining the two fluxes of Eq. 10, the particle exchange rate equations are:

$$\frac{d(N_l + N_g)}{dt} = 0 \quad ; \quad \frac{dN_l}{dt} = \beta(-\Phi_{vap} + \Phi_{cond})S_l \quad (12)$$

where S_l is the surface area of the drop and $0 < \beta < 1$ the *sticking coefficient* that is usually assumed of order 0.5. A recent study [44] has proposed a simple expression for β that is in good agreement with MD calculations for several simple fluids. This expression depends only on the ratio of the molecular volumes in the liquid and vapor phase: $\beta = (1 - (v_l/v_g)^{1/3}) \exp(-\frac{1}{2} \frac{1}{(v_l/v_g)^{1/3} - 1})$ that we plot for our VdW model for Al on Fig. 4.b.

Concerning the energy fluxes, the first equation comes from the assumption of adiabatic expansion of the cell:

$$\frac{d(E_l + E_g)}{dt} = -P_g \frac{dV}{dt} \quad (13)$$

In this global energy loss rate we have neglected three terms that could be added in a near future. The first one is heat conduction between cells. This term may play a role, but it cannot be very important as we are considering a supersonic flow (see Section I). The second neglected term is radiation. Radiation becomes indeed the dominant cooling mechanism at long times, as we will see later, but it is negligible for the initial dynamics, so the approximation is reasonable, because our purpose in this paper is to study the expansion in a time range where the two phases are interacting and the system is not just a collection of isolated clusters flying in vacuum. The third neglected term is thermionic emission. One expects electrons to be thermally emitted from the droplet, taking away some energy. Non-neutral effects are totally absent from our model, but we expect that the associated cooling rates will be small compared to the adiabatic and evaporative cooling rates [52].

The energy exchange rate between the liquid and the gas has contributions from the three fluxes of Fig. 4.a. The contribution of the colliding but non-sticking particles can be described with a flux proportional to the temperature difference $T_g - T_l$, with a relaxation coefficient

$0 < \alpha < 1$ (see e.g. [45] for more discussion). For the condensing gas particles, we make the simplest assumption, that each of them brings to the liquid the average gas energy $e_g = c_v T_g - a n_g$. For the evaporating particles, we assume that the energy they individually take away from the liquid depends only on the liquid state. We note it $e_g^* = c_v T_l - a n_g^*(T_l, R)$ because it corresponds to the energy of a virtual gas particle that would be in equilibrium with the drop of radius R at temperature T_l . This justification is totally analogous to the Hertz-Knudsen derivation of the mass evaporation rate of Eq. 12. We finally get the exchange rate

$$\frac{dE_l}{dt} = [\beta(-e_g^* \Phi_{vap} + e_g \Phi_{cond}) + (1 - \beta) \alpha c_v (T_g - T_l) \Phi_{cond}] S_l \quad (14)$$

Our set of kinetic equations is fully consistent in the sense that at equilibrium both mass and energy fluxes between the drop and the gas are in balance. Note that the energy that an evaporating particle needs to take from the liquid is $e_g^* - e_l = -a(n_g^* - n_l)$, which corresponds exactly to the latent heat (Eq. 4), without the second (work) term, which is expected since the latent heat is an enthalpy and we are here dealing with energy exchanges at constant volume.

To our knowledge, our set of rate equations is an original model for the exchanges between a drop and its vapour. Other systems of kinetic equations can be found for analogous systems (see e.g. [46, 47]), but they do not correspond to the purely kinetic regime that we are considering, because they deal with larger drops ($R > 1 \mu\text{m}$) and longer time scales, more relevant to the fields of combustion or atmospheric sciences, so they need to combine the kinetic approach with the more classic hydrodynamic theories of droplet evaporation [48].

Our model for WDM situations is simpler, because we do not distinguish in the gas a Knudsen layer *vs* a hydrodynamic layer. We assume that our computing cells are small enough that the gas density inside them is constant. The variations over the whole flow shall instead be treated by the global hydrodynamic code that determines the expansion of each kinetic cell. The kinetic and phase change processes in our description are driven by the hydrodynamic expansion, therefore, the validity condition of our model is that the initial cell size should be much smaller than the initial sample dimensions:

$$L_0 \ll \delta r, \delta z \quad (15)$$

so that the global hydrodynamic treatment is correct, with gradients properly resolved. This is verified in the standard situations we consider, but can break down if the initial droplet size is too big compared to the sample size.

C. Equilibrium condition between droplet and gas

In order to get a closed system of equations for particle and energy fluxes, we still need one assumption. Our model is a priori out of thermal equilibrium ($T_l \neq T_g$), so the density of the liquid is not determined yet. It seems reasonable to assume pressure equilibrium between the drop and the gas, because, given a certain gas temperature and density, it requires only a few collisions for the drop to "experience" the gas pressure, and adjusting the liquid pressure to it requires only a small density change, because the liquid has a very low compressibility.

Due to the drop curvature, the pressure equilibrium condition is the Laplace equation

$$P_l - P_g = \frac{2\sigma}{R} \quad (16)$$

An exact numerical implementation of Eq. 16 is difficult, because it requires to solve a non-linear system at each timestep in order to determine the liquid density given a certain set of values $\{V, N_l, N_g, E_l, E_g\}$.

To simplify the condition, one can approximate the liquid density by the equilibrium value $n_l^*(\infty)$ for a flat interface ($R \rightarrow \infty$), but this is wrong for two reasons. First, because due to the fast expansion, the gas pressure is lower than the corresponding saturation value, and second, because of the Laplace compression term of Eq. 16. Running our model, we have checked that this raw approximation leads to important inaccuracies in the calculation of the pressure, especially at low temperatures where the Laplace term becomes dominant. Still these errors do not cause important discrepancies in the global description of the drop evolution, due again to the low compressibility of the liquid.

For more accuracy, we have chosen to compute the liquid density in perturbation from the flat equilibrium value

$$n_l = n_l^*(\infty) \left(1 + \frac{\Delta P}{K_l(T_l)}\right) \quad (17)$$

where $K_l(T_l) = n_l(\partial P / \partial n_l)_{T_l}$ is the isothermal bulk modulus of the liquid that we compute directly from the VdW EoS, and $\Delta P = 2\sigma/R - (P_l(n_l^*(\infty), T_l) - P_g)$ is the pressure correction that we compute using Eq. 16. As we show in the next section, this perturbative approach of the pressure equilibrium condition is very satisfactory.

With Eq. 9-17, we have a complete model for the evolution of a droplet in an adiabatic expanding lagrangian cell. In the following, we use this model to study the different regimes of two-phase expansion.

IV. RESULTS

A. NDCX II reference case (subcritical case)

The reference case envisioned as an upcoming experiment on the NDCX II machine at LBNL consists in heating an aluminum foil of thickness $\delta z = 3.5\mu\text{m}$ with a short pulse of ions (see Table I). The beam profile is taken as a uniform disk of diameter $\delta r = 1\text{mm}$. Initial temperatures up to 1eV are predicted for the expected beam fluences [23].

On Figure 5, we present the numerical output of the model for a cell containing a droplet and gas initially at equilibrium at $T_0 = 8000\text{K}$ with $V_l = V_g = V/2$, because this corresponds to the onset of the "droplets regime" (see section II). As we mentioned previously, we make the crude assumption of a flow with linear speed profile and outward expanding speed $v_0 = 3cs_0 \simeq 5.0\text{km/s}$ on both sides $z > 0$ and $z < 0$, where the sound speed cs_0 is estimated roughly as the thermal velocity $v_{th}(T_0) = \sqrt{k_B T_0 / m}$. Then, the strain rates in Eq. 9 are simply $\eta_z = 6cs_0 / \delta z$ and $\eta_r = 6cs_0 / \delta r$. We display a full 3D case (solid lines) and a 1D case (dashed) where $\eta_r = 0$. Here $t_{hydro} = 1/\eta_z \simeq 0.37\text{ns}$. The time $t_{3D} = 1/\eta_r \simeq 107\text{ns}$ can be considered as the time of the onset of the 3D regime of expansion. The calculation is carried out with $\alpha = \beta = 0.5$ and we use the variable $u = \ln(t)$ to span a wide temporal range. The result is displayed up to $t = 100\mu\text{s}$ because at this time the front has travelled over about 5cm, which is comparable with the size of an experiment. The initial droplet size $R_0 = 25.4\text{nm}$ is estimated using Eq. 1 and is consistent with observations for similar initial temperatures [13]. This size is the mean size of the liquid fragments so we are considering the evolution of a *typical droplet*.

At early times ($t < 10\text{ns}$), a fraction of the liquid is evaporated (Fig. 5.a). But this process saturates at a time t_{min} , after which the liquid fraction starts growing slowly. Then, in the purely 1D case (dashed lines), the droplet continues to grow steadily. In the more realistic situation however (solid lines), the droplet evaporates again when the 3D regime sets in, at times $t > t_{3D}$.

On Fig. 5.b, one sees that, almost instantaneously after heating ($t < 100\text{ps}$), a temperature difference $\Delta T = T_l - T_g$ is established between the gas and the droplet, and remains roughly constant throughout the expansion in the 1D case. On the contrary, in the 3D case, T_g drops quickly to almost 0 around t_{3D} , whereas T_l decreases slowly to a value around 1600K. On Fig. 5.d, we see that in both cases the liquid density remains very close to the equilibrium value. By contrast, the gas density is clearly below the binodal in the 1D case, and in the 3D case it dives deep into non-equilibrium (supersaturated) conditions.

On Fig. 5.c, we check the pressure equilibrium con-

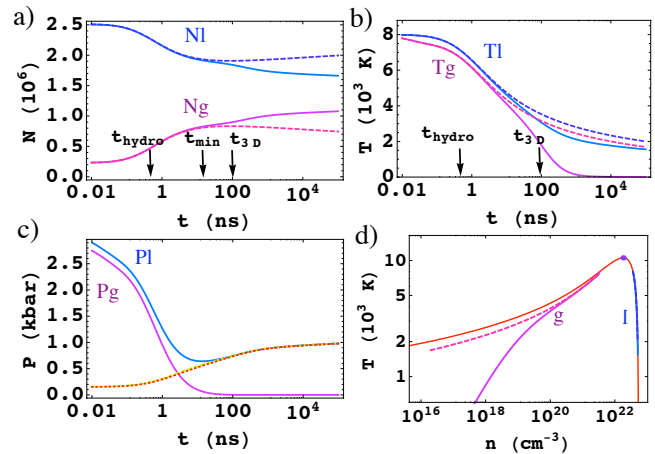


FIG. 5: Drop and gas evolution in the NDCX II reference case. Initially the drop of radius $R_0 = 25.4\text{nm}$ and the gas have equal volume and are in equilibrium at $T_0 = 8000\text{K}$. Liquid is in blue, gas in purple. Time evolution of (a) the particle numbers and (b) the temperatures, for a 1D (dashed) or a full 3D expansion (solid). (c) Pressure evolution in the 3D case. The pressure difference computed (dashed) and expected from Eq. 16 (dotted) are indistinguishable. (d) Trajectories in the phase diagram for the 1D and 3D cases

dition in the 3D expansion case. One cannot distinguish the pressure difference in the computed evolution (dashed) that uses Eq. 17 from the theoretical value of Eq. 16 (dotted), as the agreement is better than 2% over the whole simulation range. The increase of P_l at long times is due to the Laplace term (Eq. 16).

Clearly, from the NDCX II example, two different regimes can be identified. The first one, where the temperature difference is small, and remains constant, can be considered as a *quasi-thermalized regime*. In this regime the droplet grows. The second one, where the gas becomes much colder than the drop, corresponds to a *non-thermalized regime*. In this regime the drop evaporates again, as if it were in vacuum. We now discuss the various regimes.

B. Thermalization condition, quasi-thermalized regime

Let us now find a thermalization condition. In our equations, the energy is extracted from the system only by the adiabatic expansion of the gas (Eq. 13) and the gas quenching is then transmitted to the liquid via the liquid-gas energy exchange term (Eq. 14). Therefore, we should compare those two energy fluxes to find the thermalization condition.

Let us assume a small temperature difference $\Delta T/T \ll 1$, so that we are in the *quasi-thermalized* regime of expansion, as in the 1D case of Fig. 5. From Fig. 5.a, one

sees that N_l and N_g are almost stationary if $T_l \simeq T_g$. Hence, let us make the approximation $\Phi_{vap} = \Phi_{cond}$ (more precisely, $|\Phi_{vap} - \Phi_{cond}| \ll \Phi_{cond}$).

The ratio between the two energy fluxes can be estimated as follows. Let us consider a cell containing fixed numbers N_l and N_g of liquid and vapor atoms, and let $x = N_l/N_{tot}$ be the liquid fraction in the cell. In the low T limit, a small energy change can be written $dE_g = N_g \frac{3}{2} k_B dT_g$ for the gas and $dE_l = N_l \frac{5}{2} k_B dT_l$ for the liquid, according to Eq. 7. Noting $dE_{tot} = dE_l + dE_g$ the total energy lost by the cell, we define $\xi = dE_l/dE_{tot}$. Requiring stationary ΔT (i.e. $dT_l = dT_g$), we obtain $\xi = 5x/(2x + 3)$.

In the low T limit, the adiabatic cooling of the gas implies: $dE_{tot}/dt = -P_g dV/dt = -n_g k_B T_g \tilde{\eta} V_0$, where we define the volume strain rate $\tilde{\eta} = d(V/V_0)/dt$. Note that, in the 1D expansion regime, $\tilde{\eta} = \eta_z$, whereas in the 3D expansion regime, for $t \gg t_{3D}$, $\tilde{\eta} \simeq 3\eta_z \eta_r^2 t^2$ and diverges. The power transferred from the liquid to the gas is: $dE_l/dt = n_g \sqrt{k_B T_g / 2\pi m} S \chi c_v \Delta T$, where $\chi = \beta + (1 - \beta)\alpha$. To get this expression we have computed the contributions from the three terms in Eq. 14 and used $\Phi_{vap} = \Phi_{cond}$. Expressing $S = 4\pi R^2$ and $V_0 = 2 \times \frac{4}{3} \pi R_0^3$, the balance between the fluxes $dE_l = \xi dE_{tot}$ finally yields

$$\frac{\Delta T}{T} = \frac{\xi \tilde{\eta} 4\sqrt{2\pi}}{\chi} \frac{R_0^3}{v_{th}(T_g) R^2} \quad (18)$$

where we note $v_{th}(T_g) = \sqrt{k_B T_g / m}$ the thermal speed in the gas. With the approximation $R_0 \simeq R$ and neglecting the prefactors of order unity, we see that $\Delta T/T$ is simply proportional to the drop radius and the volume strain rate

$$\frac{\Delta T}{T} \sim \frac{\tilde{\eta} R_0}{v_{th}(T_g)} \quad (19)$$

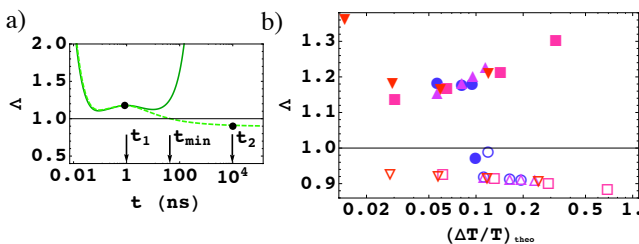


FIG. 6: Test of the thermalization formula Eq. 18. (a) Time evolution of the ratio $\Lambda = (\Delta T/T)_{theo}/(\Delta T/T)$ of the temperature difference computed with Eq. 18 to the numerical model in the NDCXII reference case, in purely 1D (dashed) and full 3D (solid) expansion. (b) Λ in the 1D expansion at $t_1 = 1$ ns (filled symbols) and at $t_2 = 10\mu s$ (hollow symbols) with $\beta = 0, 0.2, 0.4, 1$ (circles), $\alpha = 0, 0.2, 0.4, 1$ (up triangles), $\delta z = 1, 2, 4, 8\mu m$ (squares) and $R_0 = 5, 10, 20, 40$ nm (down triangles).

On Figure 6 we check the validity of Eq. 18, computing the ratio $\Lambda = (\Delta T/T)_{theo}/(\Delta T/T)$ of the theoretical temperature difference (Eq. 18) to the result of the full numerical calculation. To evaluate Eq. 18 we take the values of $\tilde{\eta}$, R , T_g and x from the result of the numerical simulation. On Fig. 6.a, we show the evolution of the ratio Λ in the NDCXII reference case (same calculation as Fig. 5). In the full 3D expansion case (solid line), the prediction becomes bad (error larger than 100%) at $t \simeq t_{3D}$, which is expected since the volume expansion rate $\tilde{\eta}$ diverges in 3D. In the purely 1D expansion, after the first ns, one sees that Eq. 18 is accurate within 20%. More precisely, the error has the same sign as the derivative dN_l/dt and vanishes when the drop is stationary, at $t = t_{min}$, which is expected since Eq. 18 is obtained with the assumption $dN_l/dt = 0$.

On Fig. 6.b, we show the ratio Λ at $t_1 = 1$ ns and at $t_2 = 1\mu s$ for the same parameters, but varying one by one those that are relevant to Eq. 18: β , α , δz (in order to vary η) and R_0 . The analytic formula overestimates (resp. underestimates) $\Delta T/T$ in all cases at t_1 (resp. t_2), and for both cases the error is larger when the expected $(\Delta T/T)_{theo}$ is larger, which is natural since Eq. 18 holds in the limit of small $\Delta T/T$. Interestingly, the point $\beta = 0$ is separate from the others at both times, and is closer to 1, which is not surprising since $\beta = 0$ means no particle exchange, and this again confirms that the main source of inaccuracy of Eq. 18 is a non-zero value of dN_l/dt . The prediction could thus be refined if this effect was taken into account, for example using the analytical results of the next section. At early times, one can see also that the error is larger for drops of radii smaller than 5nm. This effect is switched off if we set $\sigma = 0$, confirming that it is caused by surface effects.

It is also possible to rewrite Eq. 19 in terms of the initial conditions: considering $\eta \sim cs_0/\delta z$, one gets the very simple scaling law: $\Delta T/T \sim R_0/\delta z$. This last expression is only valid in the case of a 1D linear expansion where $\tilde{\eta}$ is constant. In this case, one sees using Eq. 1 that $\Delta T/T$ is expected to decrease slowly when the initial sample size increases

$$R_0 \propto \eta^{-\frac{2}{3}} \Rightarrow \frac{\Delta T}{T} \propto \eta^{\frac{1}{3}} \propto \delta z^{-\frac{1}{3}} \quad (20)$$

For larger samples, the thermalization will be better even though the droplets are bigger. This justifies again that in the limit of large samples and slow expansions, an equilibrium hydrodynamic description becomes valid.

In summary, Eq. 18 is expected to be always a good estimate in the quasi-thermalized regime, and Eq. 19 can be considered as a universal criterion to delimit the quasi-thermalized regime.

C. Fully thermalized regime

In the previous section we could distinguish the regimes of quasi-thermalized versus non-thermalized expansion. From Eq. 18 it is clear that the quasi-thermalized regime will become quickly invalid after t_{3D} , because the volume strain rate $\dot{\eta}$ diverges. Nonetheless, in the early times of expansion, or if one is interested in systems of large radial extent, it is worth studying the limiting case of a fully thermalized flow.

In this perspective, let us assume $T_l = T_g = T$. Again, we look at the low T regime, which becomes valid very early in the expansion process. Using the first order approximations $n_l \simeq (1-\theta)/b$ and $n_g \simeq 0$ (Eq. 5 and 6) and neglecting the surface energy term, we write the total energy $E_{tot} = N_{tot}(c_v T - x(1-\theta)a/b)$, where $x = N_l/N_{tot}$ is still the liquid fraction in the cell.

The total energy change $dE_{tot} = -P_g dV$ becomes, at first order in θ : $-(1-x)\theta \frac{dV}{V} = (\frac{3}{2} + x) d\theta - dx$. Noting that $dV \simeq dV_g$, we convert $\theta d(\ln(V)) = d\theta - d\theta/\theta$ using the low T approximation Eq. 6, and find finally

$$dx = \left(\frac{5}{2} - \frac{1-x}{\theta}\right) d\theta \quad (21)$$

It is easy to push the approximation to higher orders in θ , but Eq. 21 already allows one to get good insight into the evolution of the droplet. One sees that the droplet will be stationary at a temperature satisfying $\theta_{min} = \frac{2}{5}(1-x)$ corresponding to the time t_{min} already mentioned, it will evaporate before this point, for temperatures $\theta > \theta_{min}$, and grow after it, for $\theta < \theta_{min}$. This sequence is in agreement with the NDCX II reference case shown on Fig. 5. Note that, at long times, and independently from the EoS, droplets will always grow in a thermalized situation. This is due to the fact that adiabatic expansion of a perfect gas is an algebraic trajectory in phase-space ($T \propto \rho^{2/3}$), whereas Clausius-Clapeyron law predicts an exponential curve for the gas binodal, meaning that the gas in a two-phase expanding cell will always tend to saturate and make the liquid fraction grow.

On Figure 7, we show the exact numerical calculation of the thermalized evolution of a droplet whose initial radius is $R_0 = 25\text{nm}$ and for initial temperatures ranging from 7000 to 10000K. In the thermalized case, the time evolution is irrelevant, that is why on Fig. 7.a and b the temperature and liquid fraction are plotted as a function of the volume expansion ratio V/V_0 . An expansion remaining in the thermalized regime over 10 orders of magnitude volume expansion is unrealistic in the case of NDCX II, but for generality it is interesting to study this limiting trend.

On Fig. 7.c, the numerical liquid fraction versus temperature is compared to the solution of Eq. 21, starting when the volume has expanded by one order of magnitude. The analytic approximation is accurate within 20%. This shows that Eq. 21 can be used to make good

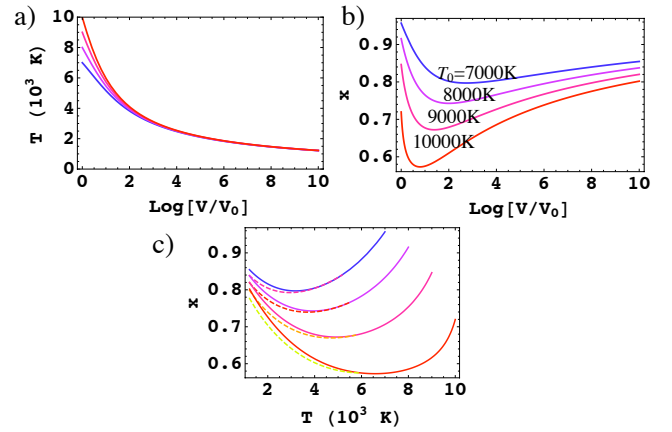


FIG. 7: Thermalized evolution for a droplet of initial radius $R_0 = 25\text{nm}$ and initial temperatures $T_0 = 7000$ to 10000K (solid lines). Temperature (a) and liquid fraction (b) evolution versus the cell expansion. (c) Full numerical calculation compared to solution of Eq. 21 (dashed) started at $V/V_0 = 10$.

estimates of the asymptotic growth of the liquid fraction in the thermalized case, which can be, for example in the case $T_0 = 9000\text{K}$, of a bit more than 10%.

This growth of the liquid fraction in the thermalized regime is a rigorous upper bound for droplet growth. In the opposite regime, one can get the reciprocal upper bound for droplet evaporation.

D. Non-thermalized regime: evaporation in vacuum

If the gas expands too fast for thermalization to occur, one expects the drop to evaporate as if it were in vacuum. The corresponding limit consists in assuming $\Phi_{cond} = 0$. Obviously, in this case the droplet can only lose particles. Moreover, the evaporation of the drop is maximal in this regime, because, if there was thermalization via collisions with a gas, colder than the drop, it would be a way for the drop to lose energy without losing particles. Also, because the vapor pressure decreases exponentially with temperature, one expects the evaporation in vacuum to slow down fast. But, independently from the kinetics, it is clear that there must be some upper bound to the evaporation of a drop. Indeed, as every evaporating particle takes away energy from the drop (the latent heat), the drop gets colder and colder, until the evaporation is "frozen", a strict limit being that T cannot become negative.

Let us find analytic expressions for the maximal evaporation of a drop whose energy is noted E_l . Considering the evaporating particles and using Eq. 14, the energy loss can be written $dE_l = e_g^* dN_l$. On the other hand, considering the liquid, and neglecting the surface energy term, one can write $dE_l = e_l dN_l + N_l (\partial e_l / \partial T_l) dT_l$.

Equating those two expressions, one finds

$$\frac{dN_l}{N_l} = \frac{(c_v - a(\partial n_l / \partial T_l))}{a(n_l - n_g)} dT_l \quad (22)$$

Within our VdW model, using the development of n_l at first order in θ (Eq. 5), one can integrate Eq. 22 from initial T_0 and N_{l0} , yielding at the final T_l the remaining fraction

$$\frac{N_l}{N_{l0}} = \exp\left[-\frac{5}{2}(\theta_0 - \theta_l) - \frac{13}{4}(\theta_0^2 - \theta_l^2)\right] \quad (23)$$

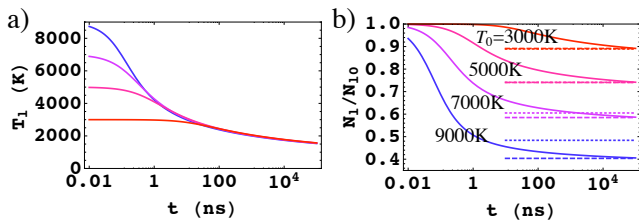


FIG. 8: Evaporation in vacuum. Time evolution of the temperature (a) and the non-evaporated fraction (b) for a droplet of initial radius $R_0 = 25\text{nm}$ and initial temperatures $T_0 = 3000$ to 9000K (solid lines). The dashed lines on (b) are the numerical integration of Eq. 22 and the dotted lines correspond to Eq. 23

Figure 8 shows the exact numerical result for the evaporation in vacuum of a droplet whose initial radius is 25nm , and initial temperatures ranging from 3000 to 9000K . The volume expansion is not relevant here, so the variables are displayed as a function of t only. On Fig. 8.a and 8.b, one sees that for all initial temperatures, the number evaporation and cooling curves of the drop follow a same asymptotic behavior, which is increasingly slow at long times. On Fig. 8.b, the numerical integration of Eq. 22 is shown for each T_0 (dashed lines), with the final T_l taken from the full numerical solution. The agreement with the final evaporation ratio is excellent, showing that surface effects play a negligible role. We have checked that surface effects cause an overestimation of the maximal evaporation of less than 10% even for droplets of initial radius 1nm . The approximated Eq. 23 is also displayed for each T_0 (dotted lines), taking here also the final T_l from the full numerical run. One sees that it predicts the good limit for evaporation within 5% for initial temperatures up to 7000K . This is very satisfactory because the non-thermalized regime is expected to be valid only in the late times of expansion so the first order low T approximations should be very accurate.

Let us now discuss the onset of the radiative cooling regime. At long times and low temperatures, the particle evaporation and the evaporative cooling rate decrease exponentially (Eq. 6), whereas the radiative cooling rate is algebraic ($\propto T^4$). Therefore thermal radiation becomes

the dominant cooling mechanism at long times. Within our model it is not difficult to express the temperature T_{rad} below which radiative cooling becomes dominant over evaporative cooling [53]. Using our VdW parameters for Aluminum, and assuming an emissivity $\epsilon = 0.2$, we find $T_{rad} \simeq 1740\text{K}$. For Si nanoparticles, the same estimate yields $T_{rad} \simeq 2190\text{K}$. This is consistent with the measurements reported in [12] where the cooling of Si nanoparticles formed by laser ablation is found to be well explained by radiation at expansion times $5 - 150\mu\text{s}$ and for temperatures below 2000K , although the evaporative cooling rates that we obtain within our model are significantly larger than the estimates they report. As an example, for Si at 2000K , our crude model predicts a radiative cooling rate of $\simeq 28\text{K}/\mu\text{s}$, while the evaporative cooling rate in vacuum is still $\simeq 6.5\text{K}/\mu\text{s}$. Note however that the rate we compute is a strict upper bound.

E. Supercritical case: nucleation and growth of liquid droplets

The last case to consider is the supercritical case, where the material expands first as a supercritical fluid, and enters the two-phase region of the phase diagram crossing the gas binodal, as a supersaturated gas. In this case nucleation of drops may occur.

We do not propose a model for nucleation but we note that it has been reported [13] that supersaturation of the vapor doesn't reach high values and that above a certain threshold value nucleation is very sudden, due to the exponential dependence of the nucleation frequency on the supersaturation ratio [32]. Then, our model is expected to describe correctly the subsequent evolution of the clusters. In particular, we expect that thermalization will depend on the values of the drop radius and the volume strain rate and that Eq. 18 will be a good estimate in the quasi-thermalized regime. If the clusters are in thermal equilibrium with the gas, Eq. 21 is expected to be valid as well.

Note that nucleation may also happen in a subcritical expansion scenario, if the gas becomes very supersaturated at long times, as can be seen for the reference case on Fig. 5.d. In this situation, close to the non-thermalized limit, condensation onto the existing droplets is too slow, and nucleation of new droplets may thus happen even if there are already liquid clusters in the plume.

V. CONCLUSION

We have studied droplet evolution and thermalization conditions with a simple kinetic model based on the Van der Waals Equation of State and a consistent set of rate equations for mass and energy exchanges. Our model

bridges the gap between the molecular and equilibrium hydrodynamic approaches that have mainly been used so far.

The VdW EoS is a simple way to model any material without much detail, but is good enough to explore the two-phase physics relevant to our problem. Although some of our analytic results are derived using specifically the VdW EoS, our kinetic model and the main results are applicable to any EoS.

The main output of our study is to identify the different regimes of two-phase expansion. On one side, the quasi-thermalized case and its limit, the fully-thermalized case, on the other side, the non-thermalized case. We propose a criterium to distinguish the two situations.

The local thermalization condition (Eq. 18) depends on the drop radius R , the volume expansion rate $\dot{\eta}$, the gas temperature T_g , the liquid fraction x , and the kinetic parameters α and β , but it can also be traced back to the initial conditions: sample thickness δz and initial temperature T_0 (Eq. 20). Eq. 19 is a simpler alternative to Eq. 18 that requires only a knowledge of the initial drop radius R_0 , $\dot{\eta}$ and T_g .

Due to the crossover around t_{3D} from 1D expansion at early times to 3D expansion at long times, the expansion is expected to take place in quasi-thermalized conditions in the early times, at least in the NDCXII reference case and for similar parameters, but at long times the non-thermalized regime is almost inevitable. Note that Eq. 18 shows that this is only a dimensional effect, because it is driven only by the divergence of $\dot{\eta}$ in 3D.

In the quasi-thermalized case, our study shows that the relative temperature difference $(T_l - T_g)/T_l$ remains almost constant throughout the expansion. Eq. 18 is derived assuming no net particle exchange, so only kinetic energy terms (but no latent heat) are involved. This makes it suitable for generalization to other EoSs, although a precise evaluation of the formula, as we have done, requires usage of the precise EoS. The predictions of Eq. 18 could also be tested with MD calculations and experimental measurements.

In the fully thermalized case, we have derived an approximate analytic expression for droplet evolution (Eq. 21), showing that drops can grow (moderately) if thermalization is maintained at long times. Eq. 21 is specific to the VdW EoS, but the general behavior is universally valid.

In the opposite scenario of a fully non-thermalized flow, Eq. 22 gives a strict upper bound for the evaporated fraction at a given final temperature, and is valid for any EoS.

For the moment, the model we have presented is local, but in the future it could become part of a larger hydrodynamic code that will treat many lagrangian two-phase cells with drops and gas inside them. The extension of our model to the case of several drops in one cell can be

done easily. It could also become necessary to include other effects that are not two-phase phenomena and that we have left aside, such as radiation, thermal conduction between cells, and thermionic emission.

A global comprehensive code will also require additional modules to compute the initial conditions. In the subcritical case, a single phase-hydrodynamic code and model for fragmentation will be needed to determine the droplets mean size and distribution at each location. In the supercritical case, a model for nucleation is required, after which our kinetic model can be used to compute the condensation and the evolution of the clusters. In any situation, the thermalization condition (Eq. 18 or 19) can be used as a test to determine if the two-phase computing cell can be treated as an equilibrium cell or if a non-equilibrium treatment is required. The reason being of course that an equilibrium (thermalized) description is much easier to implement.

The second practical use of our model is to make estimates in real situations. In particular, the limiting behaviors in the thermalized and non-thermalized cases can be used as upper bounds for the droplets' evolution. Note that, in all the cases we have studied, the droplets never grow or evaporate very much from their initial situation.

Finally, we have been able to investigate the role of surface effects in different cases. Surface tension is expected to play an important role for small drops of radii $R < R_\sigma = \sigma/k_B T n_l$. This can be seen from Kelvin equation or considering the radius at which the surface energy becomes comparable to the kinetic energy per particle in the liquid. With our VdW parameters for aluminum, R_σ increases from 0.8nm at $T = 10000\text{K}$ to 64nm at $T = 2000\text{K}$. Surface effects are thus increasingly important in the late stages of expansion, at low temperature and for the smallest fragments. This is also why a careful treatment of the supercritical case of in-flight nucleation is more difficult and remains to be done in order to complement this work.

ACKNOWLEDGEMENTS

We wish to thank R. More, F. Bieniosek, P. Seidl, and B. G. Logan for helpful discussions about droplet physics and warm dense matter. The work of one of us (JA) was partially supported by an internship at Ecole Normale Supérieure, France. Work performed under the auspices of the U.S. Department of Energy under University of California contract DE-AC02-05CH11231 at Lawrence Berkeley National Laboratory and contract DE-AC52-07NA27344 at Lawrence Livermore National Laboratory.

* Corresponding author: julienarmijo@gmail.com

- [1] R. Lee *et al.*, J. Opt. Soc. Am. B **20**, (2003).
- [2] S. Eliezer *et al.*, Phys. Rev. B **69**, 144119 (2004).
- [3] O. Albert *et al.*, Appl. Phys. A **76**, 319323 (2003).
- [4] S. Amoruso *et al.*, Phys. Rev. B **71**, 033406 (2005).
- [5] N. Tahir *et al.*, Phys. Rev. Lett. **95**, 035001 (2005).
- [6] N. Tahir *et al.*, Nucl. Instr. Meth. B **245**, 85 (2006).
- [7] P. Seidl *et al.*, Nucl. Instr. Meth. A **577**, 215 (2007).
- [8] K. Sokolowski-Tinten *et al.*, Phys. Rev. Lett. **81**, 224 (1998).
- [9] A. Lindenberg *et al.*, Phys. Rev. Lett. **100**, 135502 (2008).
- [10] N. Zhang *et al.*, Phys. Rev. Lett. **99**, 167602 (2007).
- [11] K. Oguri, Y. Okano, T. Nishikawa, and H. Nakano, Phys. Rev. Lett. **99**, 165003 (2007).
- [12] S. Amoruso *et al.*, Europhys. Lett. **67**, 404 (2004).
- [13] E. Lescoute *et al.*, Phys. Plasmas **15**, 063507 (2008).
- [14] B. Holian and D. Grady, Phys. Rev. Lett. **60**, 1355 (1988).
- [15] W. Ashurst and B. Holian, Phys. Rev. E **59**, 6742 (1999).
- [16] S. Toxvaerd, Phys. Rev. E **58**, 704 (1998).
- [17] D. Perez and L. Lewis, Phys. Rev. Lett. **89**, 255504 (2002).
- [18] D. Perez and L. Lewis, Phys. Rev. B **67**, 184102 (2003).
- [19] P. Lorazo, L. Lewis, and M. Meunier, Phys. Rev. B **73**, 134108 (2006).
- [20] A. Upadhyay and H. Urbassek, Phys. Rev. B **73**, 035421 (2006).
- [21] F. Vidal *et al.*, Phys. Rev. Lett. **86**, 12, 2573 (2001).
- [22] R. More, H. Yoneda, and H. Morikami, JQSRT **99**, 409 (2006).
- [23] J. Barnard *et al.*, Nucl. Instr. Meth. A **577**, 275 (2007).
- [24] B. Chimier and V. T. Tikhonchuk, Phys. Rev. B **79**, 184107 (2009).
- [25] D. Eder *et al.*, Nucl. Fusion **44**, 709 (2004).
- [26] A. Koniges *et al.*, J. Phys. IV France **133**, 587 (2006).
- [27] L. Landau and E. Lifschitz, Fluid Mechanics (Pergamon Press, London, 1959).
- [28] S. Anisimov *et al.*, Appl. Phys. A **69**, 617 (1999).
- [29] D. Grady, J. Appl. Phys. **53**, 010322 (1982).
- [30] E. Knuth and U. Henne, J. Chem. Phys. **110**, 2664 (1999).
- [31] M. Pilch and C. Erdman, Int. J. Multiphase Flow. **13**, 741 (1987).
- [32] S. Balibar, J. Low. Temp. Phys. **129**, 363 (2002).
- [33] M. Moody, Phys. Rev. Lett. **91**, 056104 (2003).
- [34] R. Tolman, J. Chem. Phys. **17**, 333 (1949).
- [35] A. Onuki, Phys. Rev. Lett. **94**, 054501 (2005).
- [36] A. Onuki, Phys. Rev. E **75**, 036304 (2007).
- [37] F. Reif, Fundamentals of statistical and thermal physics (MacGraw-Hill, New York, 1965).
- [38] CRC Handbook of Chemistry and Physics, edited by D. Lide (CRC Press, Boca Raton, FL, 1999).
- [39] F. Buff and R. Lovett, in Simple dense fluids, edited by H. Frisch and Z. Salsburg (Academic, New York, 1968).
- [40] V. Sarou-Kanian, F. Millot, and J. Riet, Int. J. Thermophys. **24**, 277 (2003).
- [41] H. Hertz, Ann. Phys. Chem. **17**, 177 (1882).
- [42] M. Knudsen, Ann. Phys. **47**, 697 (1915).
- [43] J. Powles, J. Phys. A **18**, 1551 (1985).
- [44] G. Nagayama, J. Chem. Phys. **118**, 1392 (2003).
- [45] M. Bond and H. Struchtrup, Phys. Rev. E **70**, 061605 (2004).
- [46] A. Kryukov, V. Levashov, and S. Sazhin, Int. J. Heat Mass Transfer **47**, 2541 (2004).
- [47] S. Sazhin *et al.*, Int. J. Heat Mass Transfer **50**, 2675 (2007).
- [48] N. Fuchs, Evaporation and droplet growth in gaseous media (Pergamon Press, London, 1959).
- [49] I. Lomonosov, Las. Part. Beams **25**, 567 (2007).
- [50] Typically, when simulating particles of mass m interacting via a Lennard-Jones potential of range σ and depth ϵ , the natural molecular time scale is $\tau = (m\sigma^2/\epsilon)^{1/2} \sim 100$ fs, see e.g. [18].
- [51] We obtain a critical temperature $T_c = 10545$ K and a critical density $\rho_c = 0.81$ g/cc whereas in [49], a comprehensive synthesis of experimental data and models leads to the estimations $T_c = 6250$ K and $\rho_c = 0.70$ g/cc for Aluminum.
- [52] Using Richardson law, one can estimate that the rate of electron emission may be high at temperatures close to T_c in the first ns of expansion. In the case where the electrons just fly away with no collisions with other drops, the energy loss for the cell is expected to be smaller than the total work term in the early times and smaller than the radiative term at long times. In addition the build-up of a charge of the drop should quickly limit the emission. In the opposite case where the emitted electrons would be recaptured by other drops, the thermionic emission and recapture terms should only amount to an increase of the thermalization rate in Eq. 14, without causing a fundamental change to the picture.
- [53] The evaporative energy flux per unit area is well approximated in the low T limit by: $\Phi_E^{evap} \simeq \beta\Phi_{vap}l_0 \simeq (\beta/b\theta)e^{-\frac{1}{\theta}}(k_B T/2\pi m)^{1/2}l_0$, while the radiative energy flux is simply: $\Phi_E^{rad} = \epsilon\sigma_S T^4$ where ϵ is the emissivity of the liquid and σ_S the Stefan constant. Finally the two processes are equally important at a temperature verifying $\theta^{-9/2}e^{-1/\theta} = (b\epsilon\sigma_S/\beta)l_0^{5/2}k_B^{-3/2}(2\pi m)^{1/2}$. To apply this formula to Si, we obtain the VdW parameters $a_{Si} = 10.1 \times 10^{-35}$ erg.cm³ an $b_{Si} = 1.68 \times 10^{-23}$ cm³ by fitting the VdW EoS to the experimental values of the latent heat $l(T_b) = 359$ kJ/mol at the boiling temperature $T_b = 3530$ K and of the liquid density $\rho_l(T_m) = 2.57$ g/cc at the melting point $T_m = 1687$ K [38], in the same way as was done for Aluminum in Section III.A.